10th ANKARA INTERNATIONAL AEROSPACE CONFERENCE **AIAC-2019-191**
18-20 September 2019 - METU, Ankara TURKEY

RANS SIMULATION BASED MULTIPOINT MULTIOBJECTIVE DESIGN OPTIMIZATION OF HELICOPTER ROTOR AIRFOIL

Onur Okumuş[1]
Turkish Aerospace
Ankara, Turkey

Alper Ezertaş[2]
Turkish Aerospace
Ankara, Turkey

ABSTRACT

A design workflow for helicopter rotor airfoil, which satisfies multiple objectives and constraints on varying flow conditions, is constructed and new rotor airfoil design sets were generated. Modern multi-point, multi-objective, design optimization algorithm available in HEEDS commercial software is utilized to search the pareto front of the design space where design variables are created with CST geometry parametrization technique. The python scripts are used for automated generation of airfoil coordinates and structured grid construction. The performance of each design candidate through the optimization workflow is evaluated by RANS simulations utilizing the Spalart Allmaras turbulence model. High fidelity simulations performed through optimization study outlines the link between the geometrical features and flow characteristics that may enable enhanced airfoils for future designs.

INTRODUCTION

The airfoil design for helicopter rotors aims maximum aerodynamic efficiency while the constraints of aeromechanic related disciplines and structural-manufacturing requirements are not hampered. The contour of the profile utilized along the rotor blade and span-wise variation of the airfoils directly define the hover and cruise efficiency in terms of power required, maximum speed attainable, useful payload that can be carried, maneuverability, noise level, vibratory loads, structural loads, control loads and autorotation capability. Due to the high aspect ratio features of the blades, state of art methods for the main rotor performance evaluation still mostly depends on theories that incorporate airfoil aerodynamic database tables. Significant improvements in rotor performance and loads can be demonstrated by improvement in the two-dimensional, static airfoil characteristics without significant modification of blade planform shapes. However, the maximum improvements in all those resulting characteristics concurrently are not attainable with single airfoil design choice, since rotor flow environment azimuthally varies and flow phenomena on different azimuthal section of the rotor disk affects different disciplines. Hence robust multi-objective multipoint design optimization framework is needed to design airfoil that can efficiently and robustly work through the varying flow environment of the main rotor.

Performance of rotor airfoil needs to be evaluated with high fidelity simulations because retreating side flow characteristics are dominated by stall while transonic effects are present

[1] Aerodynamics Design Engineer in Helicopter Group, Email: onur.okumus@tai.com.tr
[2] Aerodynamics Chief Engineer in Helicopter Group, Email: aezertas@tai.com.tr

on advancing side. Low fidelity tools such as XFOIL, MSES etc. are not competent enough in resolving shocks and stall features accurately. Thus, at least RANS simulations are needed for better resolution. Mesh independent RANS solution with validated approaches are feasible to be utilized through design work that requires large number of simulations with today's computational power. Details of followed mesh independency and validation best practices for prediction of rotor airfoil performance will be presented in full manuscript. To prevent infeasible number of design variables in design space, effective and efficient parameterization technique for geometry is required. Class-Shape Transformation (CST) method [Kulfan and Bussoletti, 2006], which is, introduced in last decade, is promising in this perspective. Scripts that are coded in python language are utilized for automation of airfoil coordinate generation and construction of computational grid. Initially, hyperbolic structured grid generation techniques based on O and C topology are utilized thorough commercial and open-source mesh generator software. Multi-Point Multi-Objective (MPMO) design is carried out within commercial HEEDS design software environment. Airfoil, which parameterized with CST method, is meshed with Pointwise and flow around it is solved with validated StarCCM+ CFD solver. In the final paper, effect of parameterization, mesh resolution and turbulence models on resulting airfoil designs will be inspected. New airfoil families will be proposed with varying the bounds of the objectives and the constraints.

Performance Requirements for Rotor Airfoil

If helicopter were only a hovering machine, maximizing the airfoils lift-to-drag ratio would be the primary requirement for the airfoil design to minimize the power required for carrying unit amount of mass through hover. Forward flight introduces asymmetric flow conditions through the rotor disk that gets worse with increasing flight speed. Hence, at forward flight conditions beyond having efficient performance through high lift-to-drag ratio rotor airfoils should also supply large operating envelope that can handle growing asymmetry on the flow conditions.

Operating envelope of a rotor airfoil can be defined by lift and drag capability change by Mach number. Maximum lift capability that can be sustained at low speeds and maximum Mach number on which airfoil can operate without significant increase of drag can be used to define the operating envelope of the main rotor airfoil. Maximum lift capability at low Mach numbers would be most demanding conditions for the airfoils at the retreating side whereas drag divergence phenomena limits the rotor performance at the advancing side. Moreover, rotor airfoils need to have low zero lift moment characteristics to minimize alternating pitch link loads due to azimuthally varying flow conditions. [Dadone, 1978] Figure 1 briefly summarizes the main requirements on airfoil that would be utilized on main rotor of a conventional single rotor helicopter. Qualitative definition of rotor airfoil requirements can be performed effortlessly i.e. high maximum lift coefficient of the airfoil would be beneficial for retreating side. However, quantification of the requirements is crucial since they are contradicting with each other and trade off analysis needed to be applied. Hence, to acquire efficient and robust rotor airfoils, MPMO type design studies that outline pareto front for contradicting objectives need to be carried out.

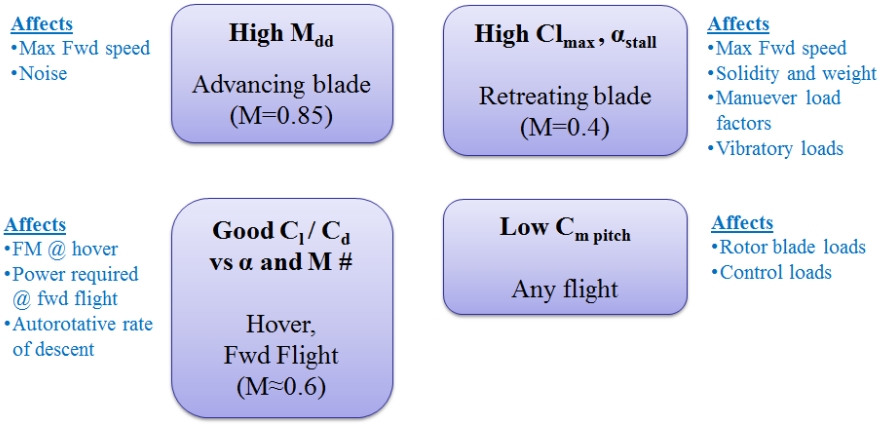

Figure 1: Requirements for helicopter rotor airfoils

METHOD

Parameterization

Way of obtaining design variables plays an important role on efficiency and success of optimization process. Broad range of parameterization methods are available, both constructive and deformative. Some of the most used methods in the literature are B-Splines, PARSEC [Sobieczky, 1999], Hicks-Henne bumps [Hicks and Henne, 1978], and Class-Shape Transformation (CST) [Kulfan and Bussoletti, 2006]. In this paper, CST method, which is widely used in aerospace field recently, is employed in the parameterization of the airfoil. CST is a powerful method that can represent the geometry with limited variables and can generate smooth curves with Bernstein polynomial. CST is formulated with class function C_{N2}^{N1} and shape function $S(\psi)$:

$$\zeta(\psi) = C_{N2}^{N1} S(\psi) + \psi \Delta\zeta_{TE}$$

Where, $\psi = x/c$, $\zeta = z/c$ and trailing edge thickness is given by ζ_{TE}.
Class function C_{N2}^{N1} is defined as:

$$C_{N2}^{N1} = (\psi)^{N1}[1-\psi]^{N2}$$

And shape functions $S(\psi)$ are defined as:

$$S(\psi) = K_i \psi^i (1-\psi)^{n-i}$$

Where the term K_i is the binomial coefficient, which is defined as:

$$K_i \equiv \binom{n}{i} = \frac{n!}{i!\,(n-i)!}$$

Round nose and pointed aft end airfoil geometries are attainable with values of N1 = 0.5 and N2 = 1.0.

Grid Generation

Generation of O and C type structured grids are automated with python scripts in initial design work. Airfoil surface discretized by 512 nodes and the initial wall spacing is set as $3.0*10^{-4}$ chord lengths to satisfy requirements of wall function approach. Unstructured mesh generated with poly type elements on StarCCM+ mesher will be included with corresponding mesh dependency on the final version of the paper with detailed investigation on near wall resolution, by satisfying y+<1 criterion. Sample of grids output by automated mesh generators are depicted in Figure 2.

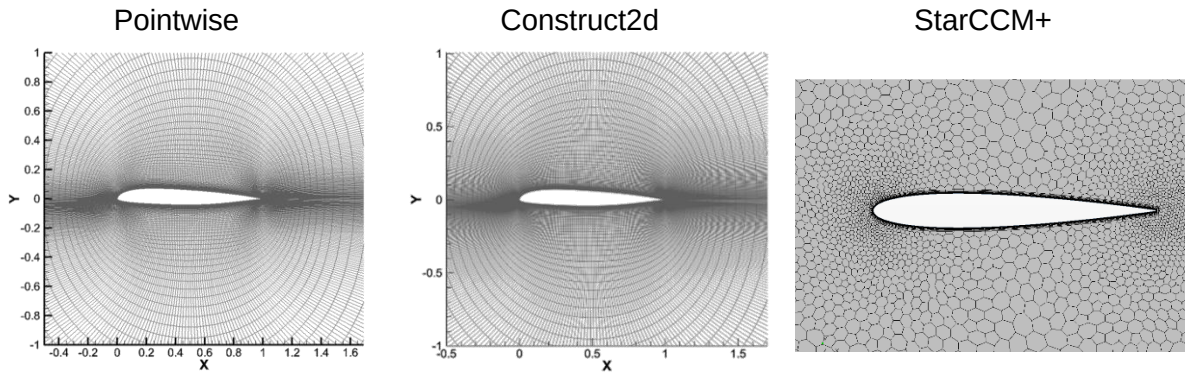

Figure 2: O type grids generated with different tools

Flow Solver

To solve the flow, StarCCM+ commercial CFD software is used. In all initial analyses, RANS flow equations with fully turbulent flow assumption are solved by using curvature corrected version of Spalart Allmaras turbulence model with wall functions. Steady, implicit density based coupled solver of StarCCM+ is used with second order spatial discretization. Inviscid fluxes are discretized by ROE Flux Difference Splitting method with Venkatakrishnan flux limiters. CFL ramping strategy and explicit under-relaxation of the equations are optimized to enhance stability of the solver to satisfy convergence within 500 iterations.

Optimization Algorithm

Multi-Objective SHERPA (MO-SHERPA) algorithm of HEEDS software is used in optimization. SHERPA is originally a single objective hybrid and adaptive algorithm. It utilizes multiple search methods simultaneously in an integrated way and adapts to the problem as optimization goes on. MO-SHERPA is multi-objective Pareto search algorithm based on SHERPA. It uses a non-dominated sorting scheme to rank designs but is quite different from NSGA-II and NCGA in other aspects. The optimization workflow driven by HEEDS is presented in Figure 3.

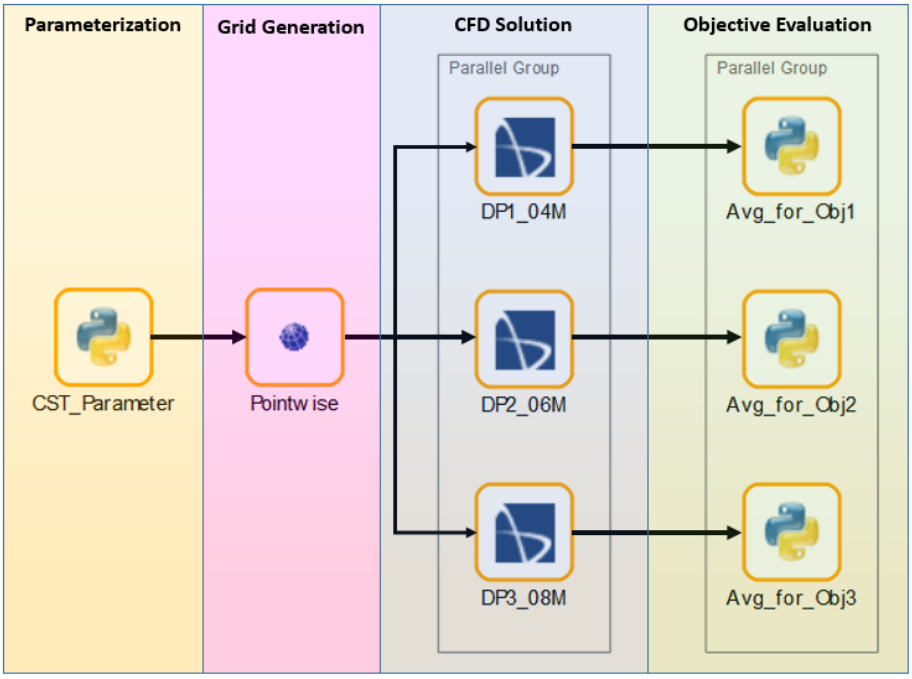

Figure 3: HEEDS airfoil optimization workflow

Design Objectives and Constraints

3 sets of multi-point, multi-objective optimization is carried out with design points, objectives and constraints chosen according to rotor airfoil design requirements as follows:

Set 1

Design Point	Design Objective	Constraint
0.4 Mach, 10° angle of attack	Maximize lift coefficient	
0.6 Mach, 3° angle of attack	Maximize lift-to-drag ratio	$\lvert C_{m,z} \rvert < 0.01$
0.8 Mach, 0° angle of attack	Minimize drag coefficient	

Set 2

Design Point	Design Objective	Constraint
0.4 Mach, 10° angle of attack	Maximize lift coefficient	
0.6 Mach, 3° angle of attack	Maximize lift-to-drag ratio	$\lvert C_{m,z} \rvert < 0.02$
0.8 Mach, 0° angle of attack	Minimize drag coefficient	

Set 3

Design Point	Design Objective	Constraint
0.4 Mach, where C_l is max	Maximize lift coefficient	
0.6 Mach, 3° angle of attack	Maximize lift-to-drag ratio	$\lvert C_{m,z} \rvert < 0.02$
0.8 Mach, where C_l is zero	Minimize drag coefficient	

This way, effect of moment constraint and the effect of design points can be seen from the comparison of the different sets. In addition, another constraint is applied for thickness to be smaller than 13% chord length. Those objectives and constraints are decided in reference to performance characteristics of the state of art, third generation rotor airfoils. Figure 4 presents airfoil performance of relevant competitor airfoils evaluated by the same CFD analysis method followed in the design study. The current design optimization study aims to attain new generation rotor airfoil families that satisfies the needs of future rotorcrafts as defined in Figure 5. [Leishman, 2007; Johnson, 2013]

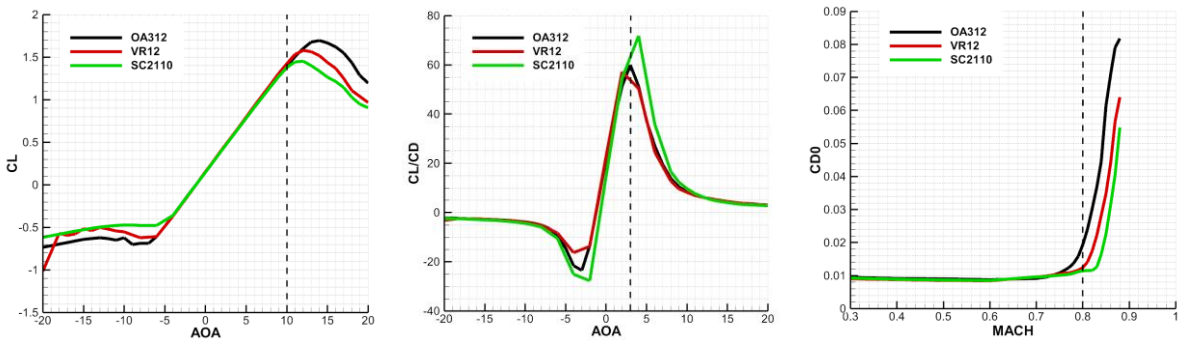

Figure 4: CFD based competitor airfoil performance charts used in selection of design points

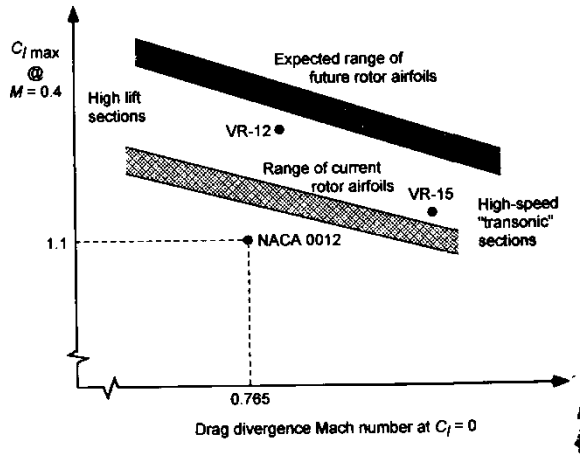

[Leishman, 2007]

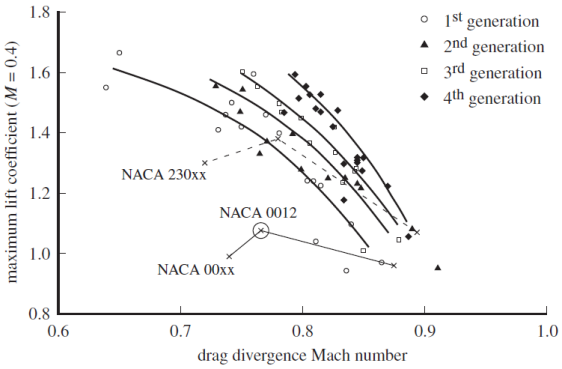

[Johnson, 2013]

Figure 5: Design targets for future rotor airfoil

VALIDATION

The validation study is conducted with the NACA0012 since there are various experiments for this airfoil. Wind tunnel data gathered for NACA0012 airfoil in [McCroskey, 1987] is used in validation. Mesh, which is shown in Figure 6, is generated with 512 points on airfoil, 7 points on blunt trailing edge and farfield is placed at 300 chord distance.

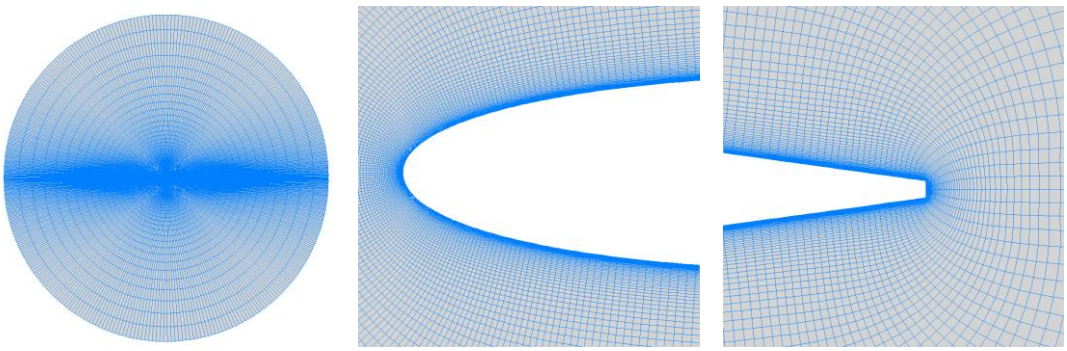

Figure 6: Mesh generated in Pointwise

To solve the flow, 3 CFD tools, Fluent, StarCCM+ and SU2 are utilized and similar models are created for each of them. Properties of the solvers are given in Table 1.

Table 1: Solver Properties

	Fluent	**StarCCM+**	**SU2**
Turbulence Model	**Spalart-Allmaras** Curvature Correction	**Spalart-Allmaras** Curvature Correction	**Spalart-Allmaras**
Solution Scheme	Pressure Based - Coupled (Pseudo Transient)	Density Based - Coupled	Density Based - Coupled
Discretization	Pressure - Second Order Density - Third Order MUSCL Momentum - Third Order MUSCL Energy - Third Order MUSCL μ_t - Second Order	Flow - Third Order MUSCL μ_t - Second Order	Flow - Third Order MUSCL μ_t - Second Order
Boundary Conditions	TV Ratio - 1.29	TV Ratio - 1.29	--

Maximum lift coefficient, maximum lift-to-drag ratio and zero-lift drag coefficients are drawn in Figure . While maximum lift and drag coefficient show great agreement with tunnel data, maximum lift-to-drag ratio shows similar behavior with test data, but they have constant shift.

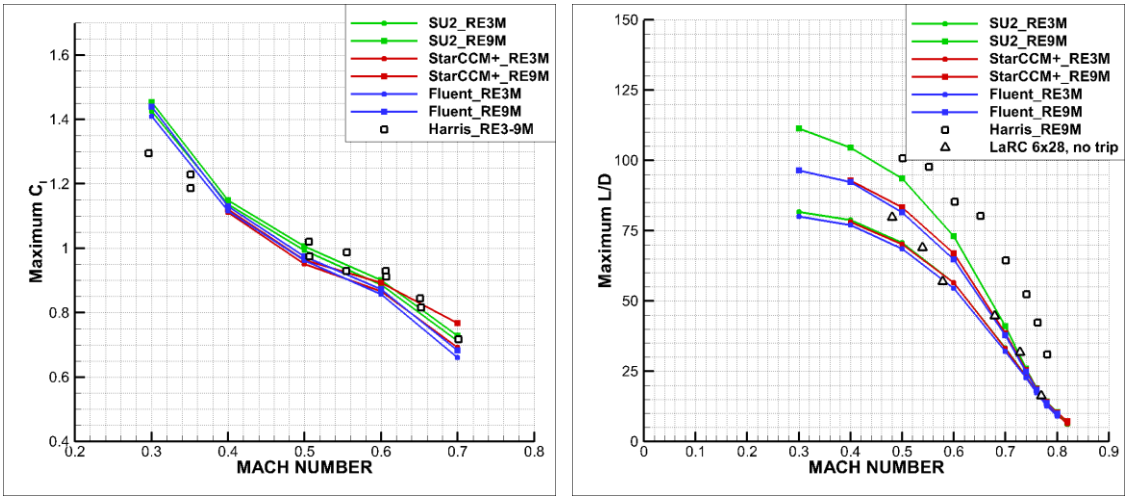

Figure 7: Wind Tunnel and SU2 results at different Reynolds numbers

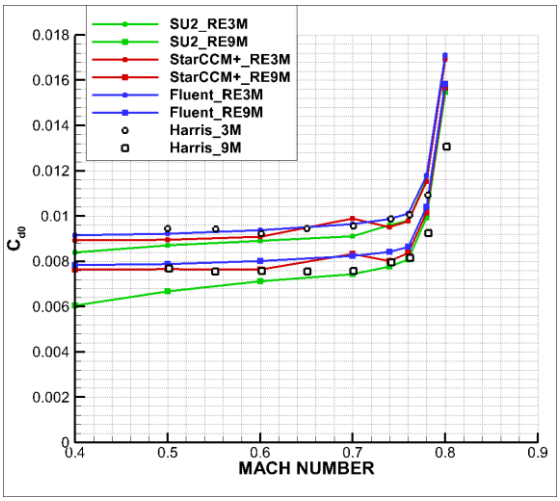

Figure 7 (continued): Wind Tunnel and SU2 results at different Reynolds numbers

RESULTS

All 3 sets are generated with 32 design iterations and total of 1024 different airfoils are assessed. Parallel radial chart depicted in Figure 8, outlines the swept discrete design space for Set 1 where each axis represents different CST parameter. Left chart shows all designs tested including infeasible designs that exceeds constraints set. After constraints applied, remaining feasible designs are drawn in the right chart and lines are colored with corresponding airfoil's lift coefficient at 0.4 Mach and 10° angle of attack. The reduction on the absolute value of lower surface and enlargement on the upper surface design variables indicates the enlargement of the camber. Comparing the feasible and infeasible designs, it is clearly observable that highly cambered alternatives are eliminated by optimization algorithm considering the constraint on moment coefficient.

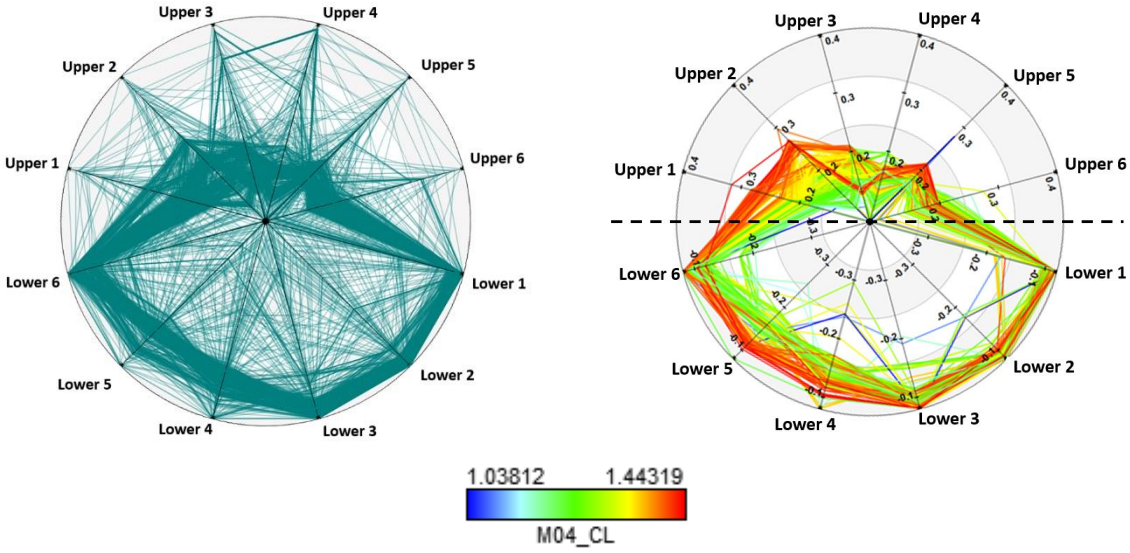

Figure 8: Feasible and infeasible designs swept through design space

Figure 9, shows each design objective variation for each feasible design alternative visited through optimization iterations. Vertical axis reflects design target set for retreating side of rotor, whereas horizontal one refers to advancing side criteria. The color of each point presents the magnitude of third objective. Hence, the alternatives with red color on the pareto front of the first and second objectives are the best considering the third objective. Some of the sample airfoils that satisfies all three objectives superiorly according to aforementioned evaluation are drawn in Figure 10 with comparison to modern, third generation helicopter rotor airfoils mentioned previously.

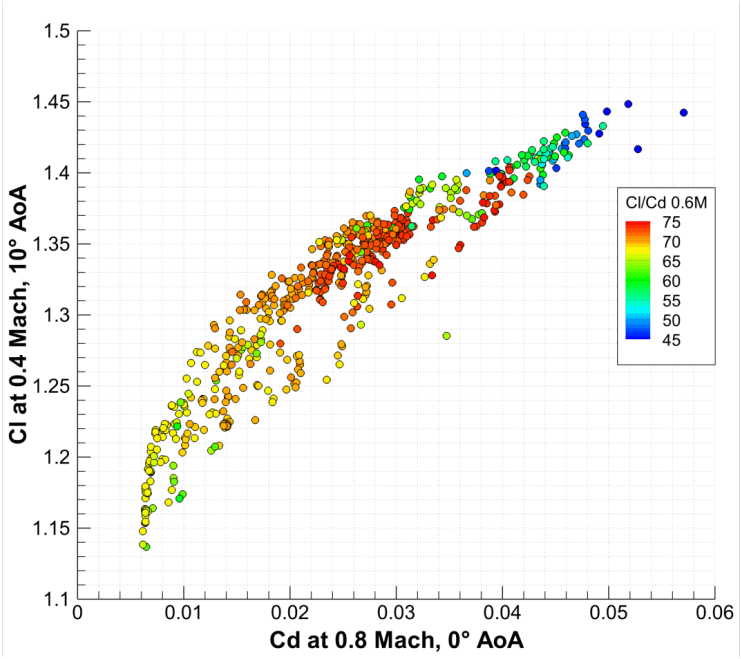

Figure 9: Variation of objective values for constraint satisfying design alternatives

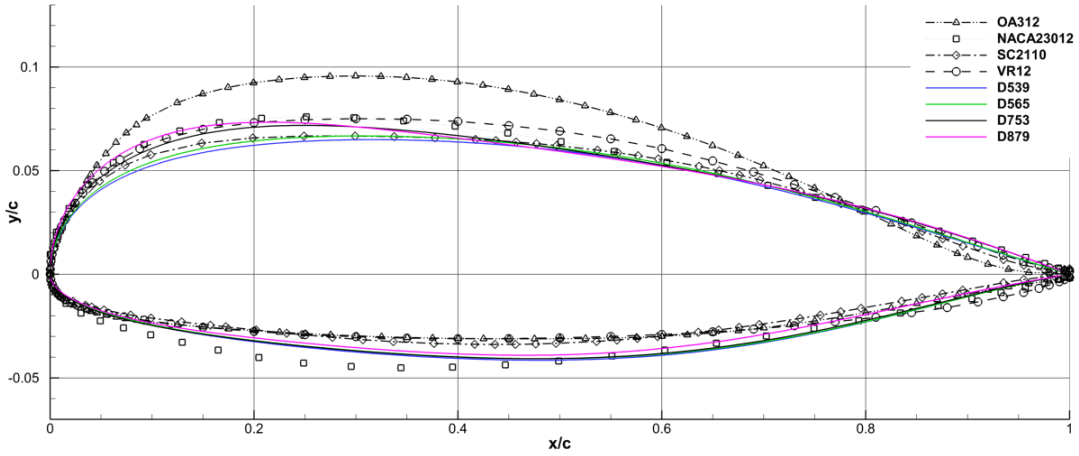

Figure 10: Resulting and third generation rotor airfoil geometries

The effect of Moment Constraint

Second set of design alternatives are generated with different moment constraint than Set 1. In Figure 11, effect of the wider moment constraint range can be observed. Airfoils generated in second set have larger lift coefficients at smaller drag coefficients with the cost of larger moment coefficient. When the airfoil shapes are compared between two sets in Figure 12, no significant differences are seen considering the design space the sets cover.

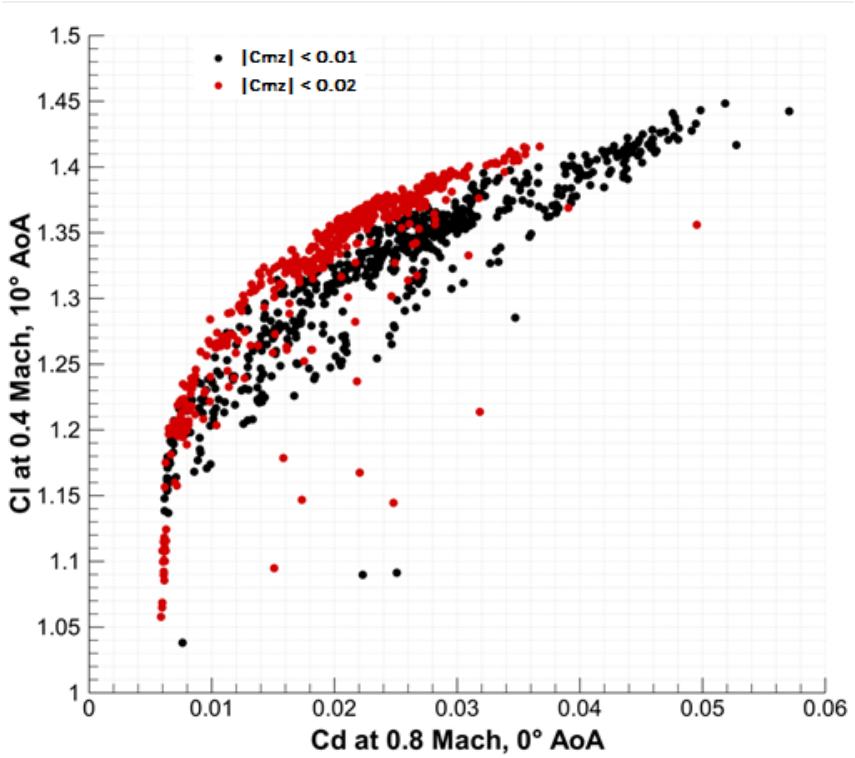

Figure 11: Comparison of the objectives of 1st and 2nd design sets

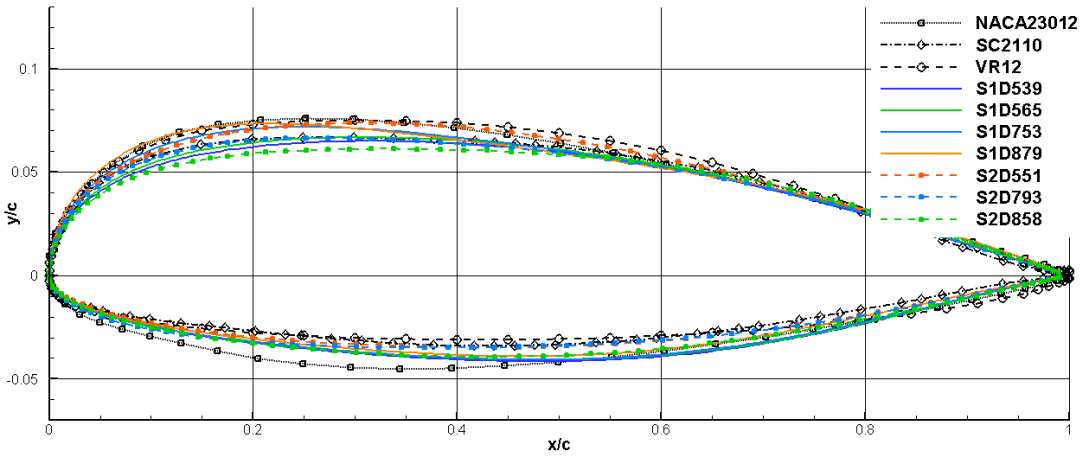

Figure 12: Comparison of the airfoil shapes of 1st and 2nd design sets

The effect of Design Points

In the third design set, significant changes are introduced on design points which had a larger impact on the shape of the airfoils. When airfoil shapes for Set 2 and Set 3 drawn in Figure 13 are compared, it shows that airfoils from third set are thicker than airfoils from both Set 2 and competitors.

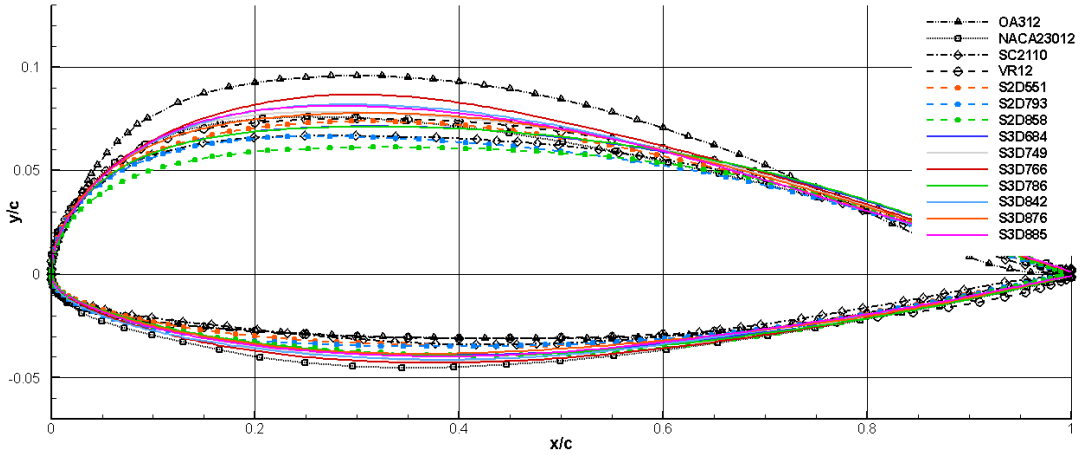

Figure 13: Comparison of the airfoil shapes of the 2nd and 3rd design sets

In-depth Examination of Set 3

Drawn airfoils in Figure 13 are chosen from the pareto front shown in Figure 14. S3D786 airfoil is the best according to Overall Evaluation Criteria, OEC, which defined as:

$$OEC = \frac{\frac{C_{l,max}}{\max(C_{l,max})} + \frac{\min(C_{d,0})}{C_{d,0}} + \frac{L/D}{\max(L/D)}}{3} \cdot 100$$

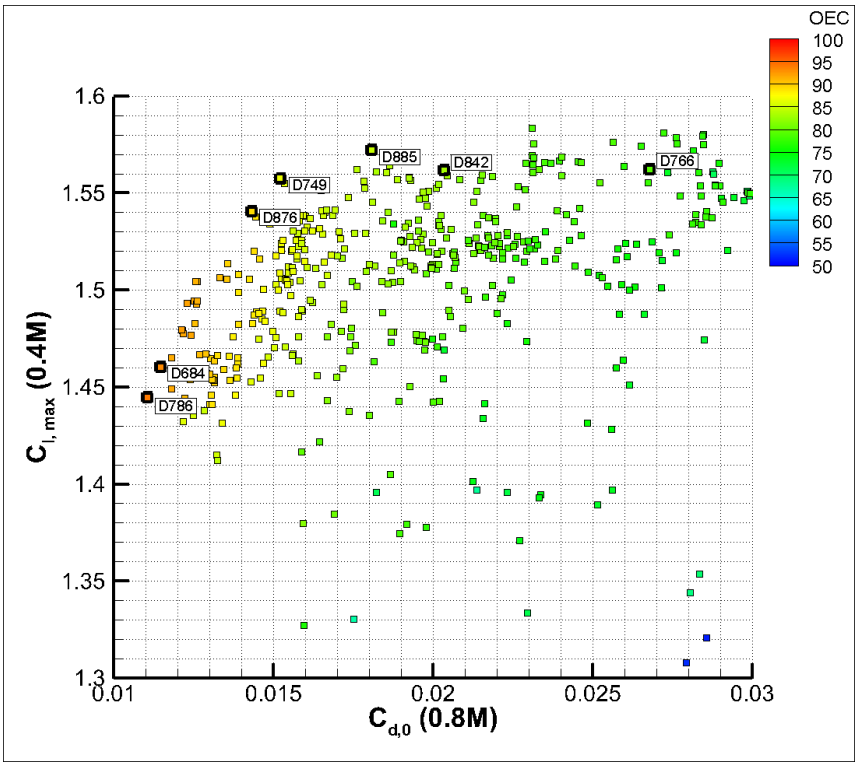

Figure 14: Variation of objective values for constraint satisfying design alternatives of 3rd set

To determine the aerodynamic characteristics of these chosen airfoils, their polar are obtained at different Mach numbers and compared with each other. Results presented in Figure 15 shows that D766 has much better lift-to-drag ratio and comparable maximum lift coefficient but lower MDD value. Airfoil with best OEC, D786, has still better lift-to-drag ratio compared to competitor airfoils but falls behind of the other airfoils in the third set. It also behaves poorly in lift coefficient but has the largest MDD value which is probably the reason behind his large OEC.

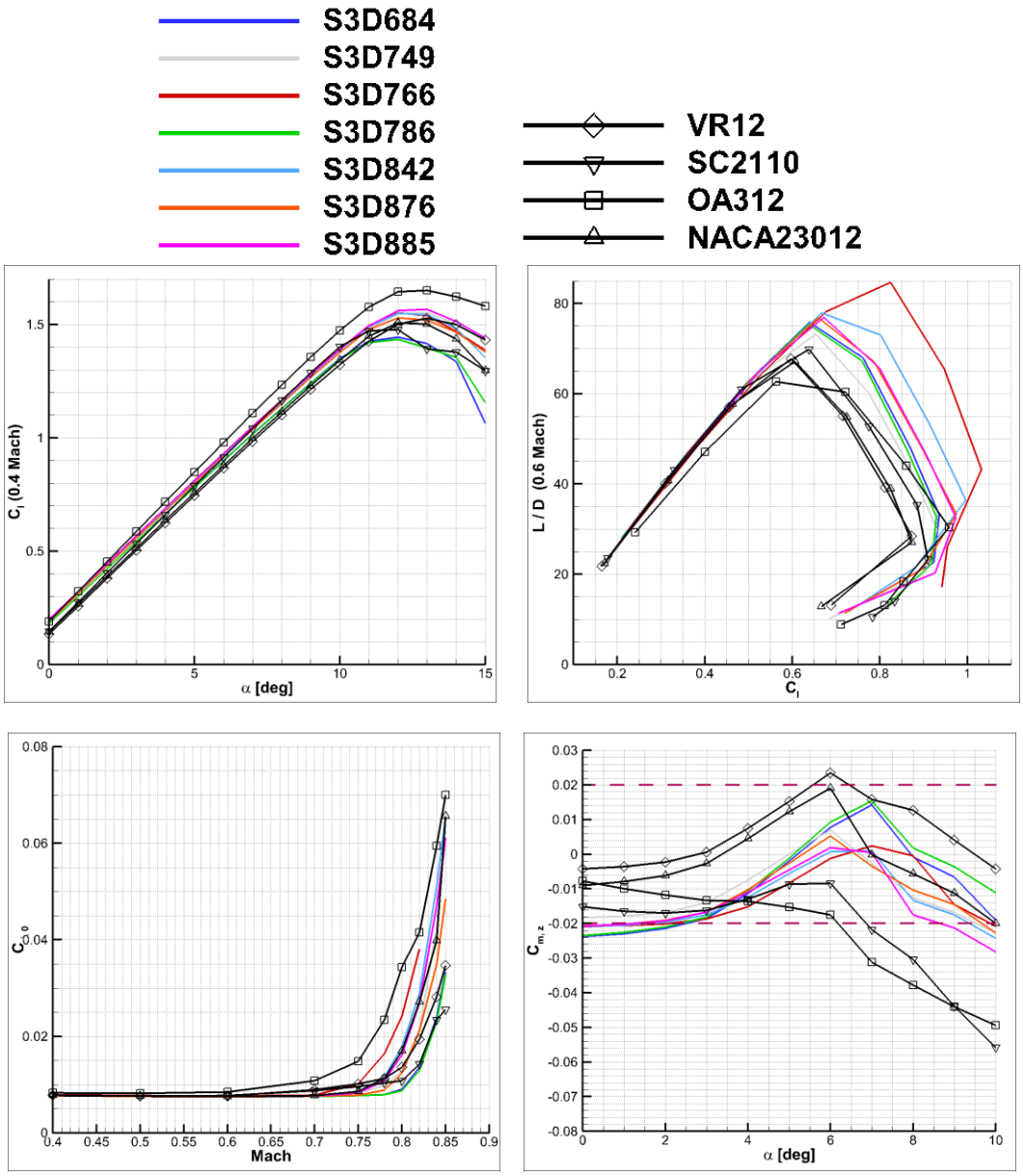

Figure 15: Comparison of aerodynamic characteristics at design points without tab

S3D766 and S3D786 airfoils shows peak performance at at least one of the objectives so they are chosen again to compare performance with a tab at trailing edge which will be added while manufacturing the main rotor. Tab with 12.5mm length and 2mm thickness is added without deforming the airfoil shape.

Before performance comparison, validation process of NACA0012 is repeated with some of the third generation main rotor airfoils VR12, SC2110, OA312 and optimization airfoils, S3D766 and S3D786 whose results are presented in Figure 16.

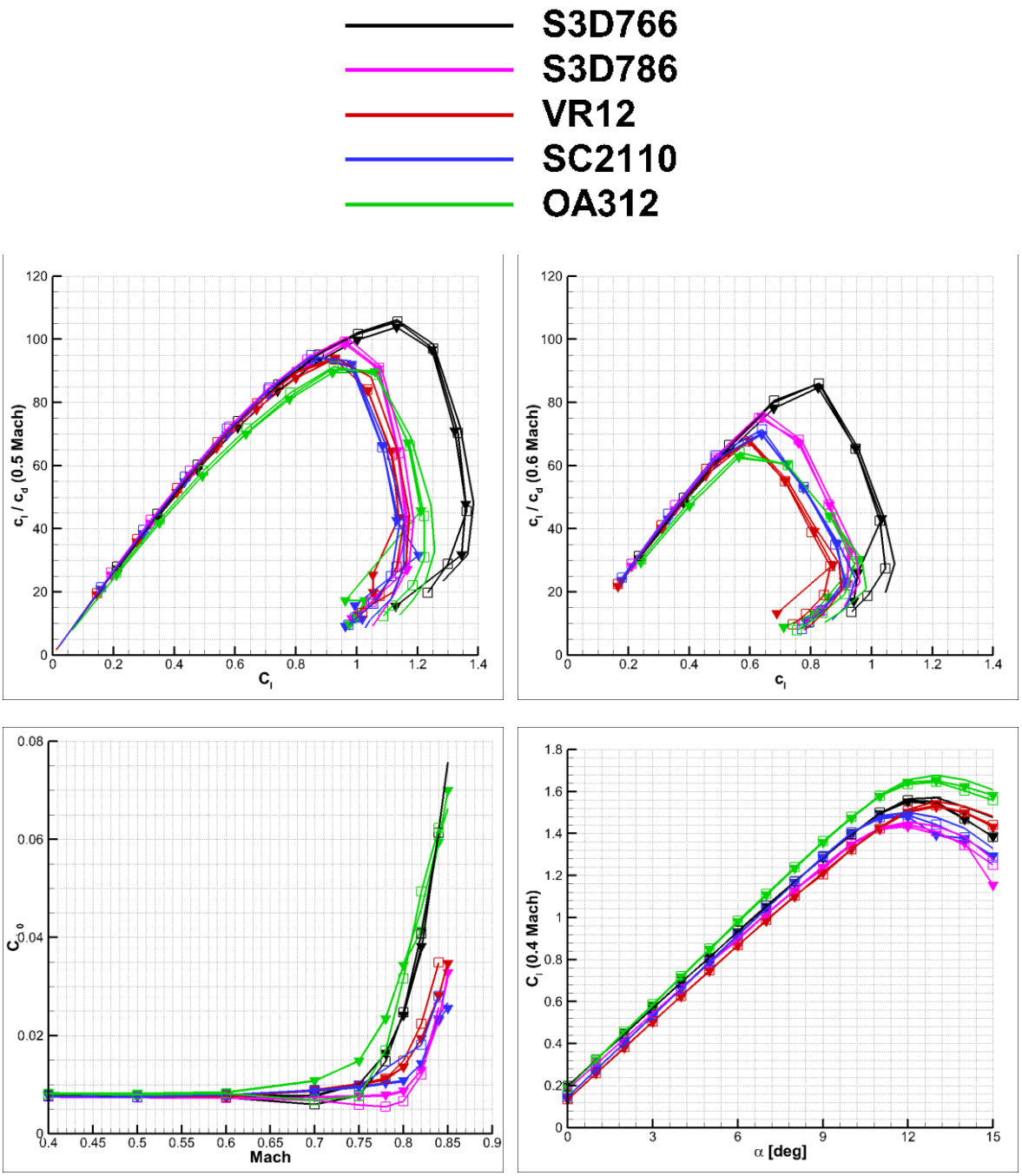

Figure 16: S3D766 and S3D786 with third generation main rotor airfoils

(SU2: no symbol, StarCCM+: Square, Fluent: Gradient)

In Figure 18, aerodynamic characteristics of airfoils drawn in Figure 17 are compared with and without tab. While lift coefficient changes at 0.4 Mach are small, lift-to-drag ratio gets

remarkable decrease with tab. Moment behavior at low angles shows improvement for optimized airfoils with tab. Design objectives calculated for the chosen airfoils are shown in Table 2.

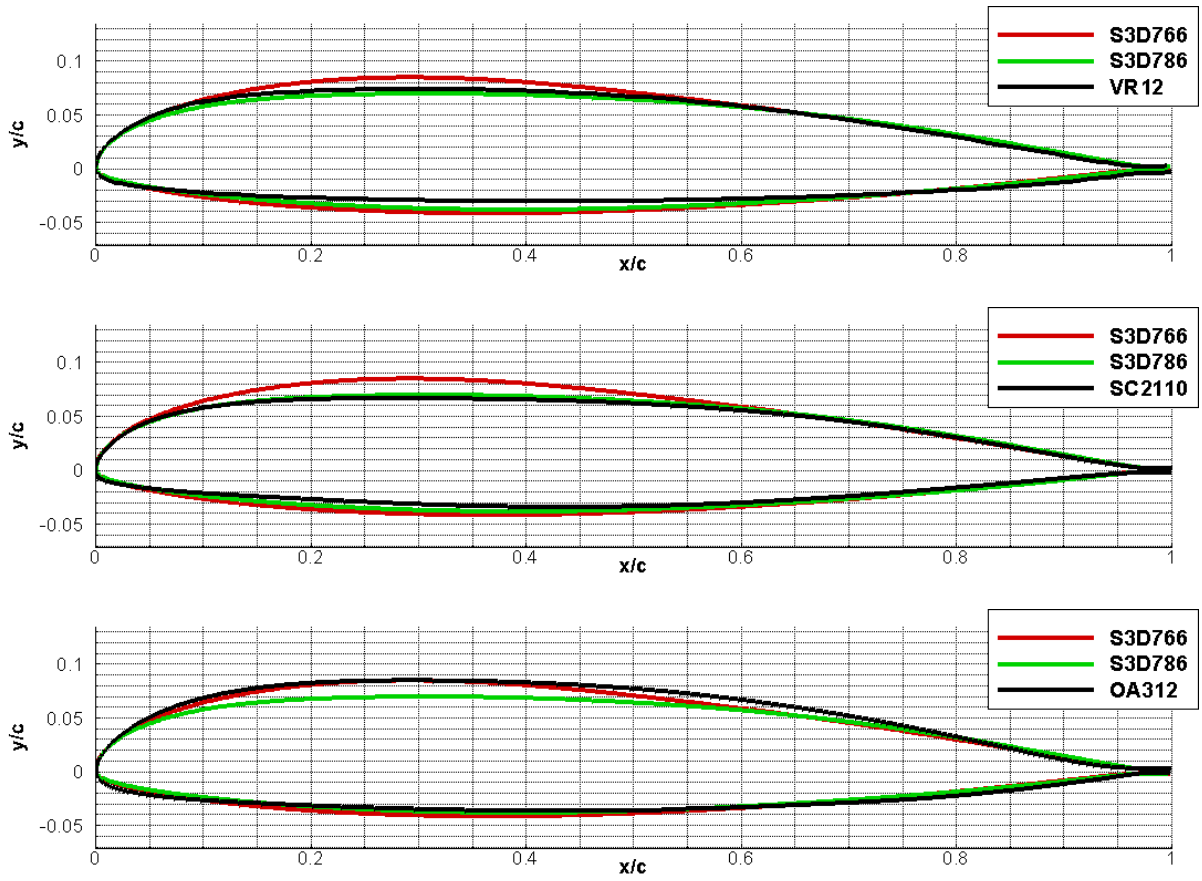

Figure 17: Chosen airfoil geometries in comparison to third generation airfoils

Table 2: Design objective values

Airfoil	$c_{l,max}$ (0.4 Mach)	c_l/c_d (0.6 Mach 3°)	M_{DD}	Thickness
D766	1.569	**76.665**	0.74	12.9% at 33%
D786	1.455	69.325	0.80	11.0% at 36%
VR12	1.566	62.115	0.78	10.6% at 35%
SC2110	1.493	57.887	0.81	9.9% at 37.7%
OA312	**1.692**	56.898	0.76	12% at 34.5%

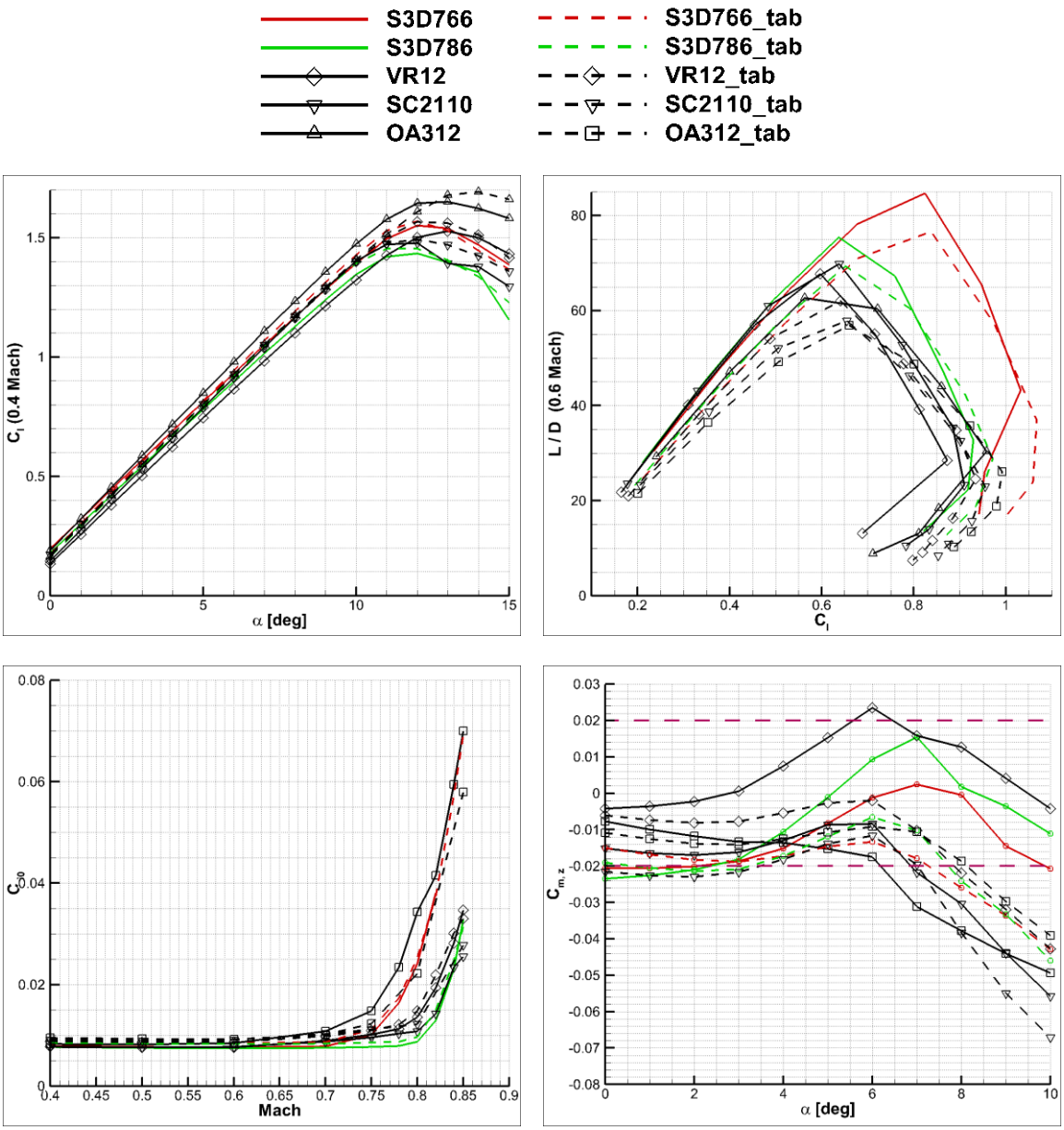

Figure 18: Comparison of aerodynamic characteristics at design points with tab

CONCLUSION

Multi-point, multi-objective design optimization process is outlined and parts of the process, generation of airfoil and grid, computation of flow field around the airfoil and optimization algorithm used with its objectives and constraints are presented in detail.

Chosen design objectives showed conflicting relations with each other such that where one showed improvement, others brought penalties with the variation of design variables. This relation created the pareto front which contains the feasible and competitive airfoils. Some of these airfoils are inspected in detail and shown that they have comparable performance with state-of-the-art third generation airfoils. Also, examining the airfoils from this pareto front showed that thickness to chord length ratio is varied between 10 to 12% and the location of maximum thickness between 20 to 40% for the airfoils on the pareto front.

Ongoing study for assessment of the rotor performance enhancement with optimized airfoils obtained by the design procedure presented in this manuscript will be elaborated in separate publication.

References

Dadone., L. U. (1978) *Design and Analytical Study of a Rotor Airfoil - NAS1-14659*, NASA, May 1978.

Hicks, R.M. and Henne, P.A. (1978) *Wing design by numerical optimization*, Journal of Aircraft Vol. 15, (7), 1978, pp. 407-412

Johnson, W. (2013) *Rotorcraft Aeromechanics*, Cambridge University Press, 2013

Kulfan, B. M, Bussoletti, J. E. (2006*) Fundamental Parametric Geometry Representations for Aircraft Component Shapes*, AIAA-2006-6948, 11th AIAA/ISSMO Multidisciplinary Analysis and Optimization Conference: The Modeling and Simulation Frontier for Multidisciplinary Design Optimization, 6 - 8 September 2006

Leishman, J. G. (2007) *The Helicopter, Think Forward, Looking Back*, College Park Press, 2007

Sobieczky, H. (1999) *Parametric airfoils and wings*, Recent Development of Aerodynamic Design Methodologies, Springer, 1999, pp 71-87